AIP | Journal of Applied Physics

Temperature-dependent local structure of LaFeAsO1−xFx: Probing the atomic correlations

T. A. Tyson, T. Wu, J. C. Woicik, B. Ravel, A. Ignatov et al.

Citation: J. Appl. Phys. 108, 123715 (2010); doi: 10.1063/1.3525999
View online: http://dx.doi.org/10.1063/1.3525999
View Table of Contents: http://jap.aip.org/resource/1/JAPIAU/v108/i12
Published by the AIP Publishing LLC.

Temperature-dependent local structure of $LaFeAsO_{1-x}F_x$: Probing the atomic correlations

T. A. Tyson,[1,2,a)] T. Wu,[1] J. C. Woicik,[3] B. Ravel,[3] A. Ignatov,[2] C. L. Zhang,[2] Z. Qin,[1,2] T. Zhou,[1,2] and S.-W. Cheong[2]
[1]*Department of Physics, New Jersey Institute of Technology, Newark, New Jersey 07102, USA*
[2]*Department of Physics and Astronomy and Rutgers Center for Emergent Materials, Rutgers University, Piscataway, New Jersey 08854, USA*
[3]*National Institute of Standards and Technology, Gaithersburg, Maryland 20899, USA*

(Received 14 July 2010; accepted 13 November 2010; published online 30 December 2010)

The local structure of the parent and doped $LaFeAsO_{1-x}F_x$ (pnictide) compounds were studied by x-ray absorption spectroscopy and density functional methods. In the doped system, the Fe–As and Fe–Fe correlations are both well modeled by an Einstein model. For the Fe–As bonds, the Einstein temperatures are identical for the doped (11%) and undoped samples but the doped sample is found to have a lower level of static disorder. Doping is found to increases the effective Einstein temperature of Fe–Fe atomic correlation. The results suggest that the onset of superconductivity in the F doped system may be related to enhanced magnetic interactions. Density functional calculations of the total charge density reveal strong bonding between neighboring As ions but metal-like behavior in the Fe layers. It is also seen directly that the replacement of oxygen by fluorine modifies the electron charge density mainly on the Fe sites. © *2010 American Institute of Physics*. [doi:10.1063/1.3525999]

I. INTRODUCTION

With the discovery of superconductivity in the non copper based pnictide system $LaFeAsO_{1-x}F_x$,[1,2] much work is being conducted to unravel the mechanism behind superconductivity in this material. A fundamental understanding of the structure from the perspective of the long range (unit cell averaged) and local (local site averaged) is essential to providing the details needed to develop a microscopic level model. The parent compound (x=0) in $LaO_{1-x}F_xFeAs$ exhibits a transition from an tetragonal phase $P4/nmm$ to a orthorhombic phase *Cmma* at low temperature near ~160 K followed by antiferromagnetic spin density wave (AFM-SDW) ordering at ~145 K.[3] The most recent measurements indicate that the onset of the orthorhombic distortion occurs at ~200 K with an abrupt increase near ~160 K.[2] In the underdoped system, orthorhombic distortions are found to exist beyond the AFM phase and coexists with the superconducting phase with no evidence for static long-range AFM order below the superconducting temperature.[3] Doping with F suppresses the splitting of the (400) and (040) beyond x=0.05. The results suggest competition between AFM order and superconductivity. Diffraction based measurements[3] indicate that F doping compresses the c-axis and makes the a-axis length approach the b-axis (with respect to the orthorhombic cell). Doping with F brings the ReO and FeAs blocks closer. No abrupt change in structure in the low temperature phase is seen with doping. The resulting structural changes with doping make the Fe–As–Fe bond angle approach the value appropriate for a perfect tetrahedron of 109.5°. Local structural measurements may provide insight which will complement the unit cell averaged structure obtained by neutron and x-ray diffraction by enabling direct measurement of interactions between pairs of atoms.

To directly probe changes in the local structure about the Fe sites, x-ray absorption measurements were conducted between 15 and 300 K in the parent and doped (11%) $LaFeAsO_{1-x}F_x$ system. In the doped system, the Fe–As and Fe–Fe correlations are both well modeled by an Einstein model. While the Einstein temperatures are identical for the doped (11%) and undoped samples, the doped sample is found to have a lower level of static disorder in the Fe–As distribution. For the Fe–Fe correlation, doping enhances the effective Einstein temperature. The results suggest that the onset of superconductivity in the F doped system may be related to enhanced magnetic correlations. Density functional calculations show that F doping modifies the electronic charge density mainly on the Fe sites.

II. EXPERIMENTAL AND COMPUTATIONAL METHODS

Polycrystalline samples were prepared by solid state reaction and detailed x-ray absorption near edge studies of the trends in electronic structure with doping have been conducted indicating proper dependence on x (see Ref. 4). Rietveld refinement of x-ray diffraction data on the x=0 system reveal no detectable impurities while LaOF impurities at the levels of ~4% were detected in the x=0.11 sample. This level of impurities is consistent with previously reported work by others on the same system.[3] We note also that in the F doped system the exact F doping is difficult to determine. However, in our doped sample the resisistivity data indicate an onset of superconductivity near 23 K.

X-ray absorption samples were prepared by grinding and sieving the material (500 mesh) and brushing it onto Kapton

a)Electronic mail: tyson@adm.njit.edu.

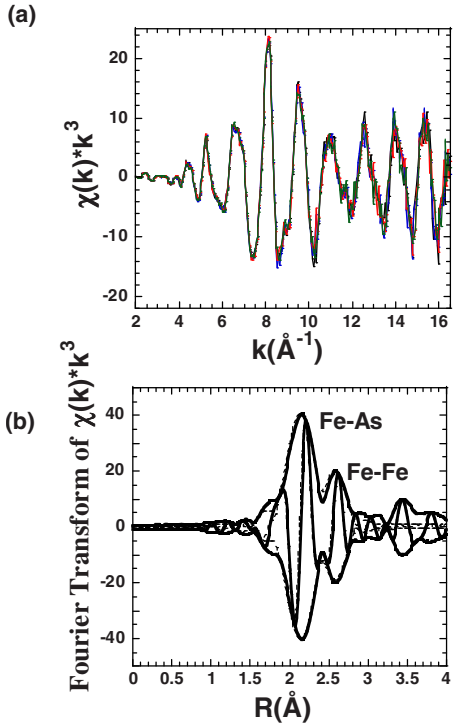

FIG. 1. (Color online) (a) Four consecutive scans at 165 K (x=0) showing the quality of the Fe K-Edge XAFS data. (b) Fourier transform of the averaged XAFS data. The dashed thin lines are fits to the data. The first and second shell Fe–As and Fe–Fe peaks are labeled. Peaks are shifted to lower R-values from real distances by atomic phase shifts.

tape. Layers of tape were stacked to produce a sample for transmission mode measurements. The stack of layers were compressed between two copper plates with a small opening [3 mm(V)×8 mm(H)] for beam access. The sample temperature sensor was attached to the plate near the sample. This approach yields very good sample temperature control as can be seen from the sharp magnetic transition features obtained for $HoMnO_3$.[5] Spectra were measured at the National Institute of Standards and Technology (NIST) beamline X23-A2 at the National Synchrotron Light Source (NSLS) at Brookhaven National Laboratory. Measurements were made on warming from 15 K in a closed-cycle Displex™ cryostat. Two to four scans were taken at each temperature. The uncertainty in temperature is <0.25 K. A Fe foil reference was employed for energy calibration. The reduction of the x-ray absorption fine-structure (XAFS) data was performed using standard procedures.[6] Representative XAFS data at 160 K are shown in Fig. 1(a). Measurement in transmission mode eliminates amplitude suppression of XAFS signals due to sample self absorption which are seen in fluorescence measurements. In addition, use of an unfocused beam on the X23-A2 NSLS beamline leads to data with very high signal to noise levels [Fig. 1(a)] with low noise for k up to 16 $Å^{-1}$. Fourier transforms of these data yield well resolved Fe–As an Fe–Fe shells [Fig. 1(b)]. Room temperature measurements were also conducted in fluorescence mode and revealed the strong loss of amplitude with low separation of the first r-space shells as found in Ref. 7. This measurement difference possibly explains the differences between results in Ref. 7 and those presented herein. Proper analysis of fluorescence XAFS data for self-absorption effects and comparison with transmission data is discussed in detail in Ref. 8, and references therein.

To treat the atomic distribution functions on equal footing at all temperatures the spectra were modeled in R-space by optimizing the integral of the product of the radial distribution functions, representing each unique shell, and theoretical spectra with respect to the measured spectra (as in Ref. 9). Theoretical spectra for atomic shells[10] were derived from the $P4/nmm$ crystal structure.[11] Both the Fe–As and Fe–Fe distributions were modeled: k-range $2.2<k<16.2$ $Å^{-1}$ and r-range $1.54<R<3.00$ Å with $S_0^2=0.80$ (account for energy loss to multiple electron excitation channels). The coordination numbers of the two shells were held at N1=N2=4 and Gaussian widths $[\sigma^2=\langle(R-\langle R\rangle)^2\rangle$ giving the mean squared relative displacement of a bond)] and bond distances for the Fe–As and Fe–Fe shells are determined. Typical XAFS data (x=0) are shown as multiple scans at 165 K in Fig. 1(a) and a typical two-shell fit in R-space is shown in Fig. 1(b). The temperature dependence of the Fe–As and Fe–Fe Debye–Waller factors (σ^2) was modeled by an static contribution (σ_0^2) plus a single parameter (θ_E) Einstein model using the functional form $\sigma^2(T)=\sigma_0^2+\hbar^2/2\mu k_B\theta_E \coth(\theta_E/2T)$,[12,13] where μ is the reduced mass for the bond pair. This simple model represents the bond vibrations as harmonic oscillations of a single effective frequency proportional to θ_E. The parameter σ_0^2 represents the static disorder. It provides an approach to characterize the relative stiffness of the bonds and can be used to ascertain changes in pair correlations. It differs from the x-ray derived Debye–Waller factor in that the latter describes motion with respect to the equilibrium position of an atom. The XAFS derived parameters directly probe the atom-atom correlations which may be relevant to magnetic interactions. In the undoped system, the coefficient $\hbar^2/2\mu k_B\theta_E$ is given by 0.0024 and 0.0032 $Å^2$ for the Fe–As and Fe–Fe bonds, respectively. The corresponding values for the doped system are 0.0024 $Å^2$ and 0.0029 $Å^2$, respectively. Errors bars on fit parameters shown represent the statistical uncertainty in the data. They are derived from the statistical spread in fits of individual scans as in Ref. 5.

To understand the difference in correlation functions for the Fe and As ions, the total charge density was examined. Calculation of the total charge density within the local spin density approximation (U/J=0) was carried out using highly accurate all-electron full potential linear augmented plane-wave plus local orbital (FPLAPW+lo) method implemented in the WIEN2K code.[14] The parent compound structure at 2 K from Ref. 3 was used. A doubled cell (a→2a) with 1/8 of the O atoms replaced by F atoms (12. 5% F doping) was used to simulate doping with F ions (with a reduced space group $P222$). An analogous calculation for the undoped system was performed and the difference charge density was obtained.

III. RESULTS AND DISCUSSION

In Fig. 2 we show the temperature dependence of the Fe–As correlation as a function of temperature for the doped and the undoped system. The Fe–As bond correlation is fit well for both the doped and undoped samples over the entire

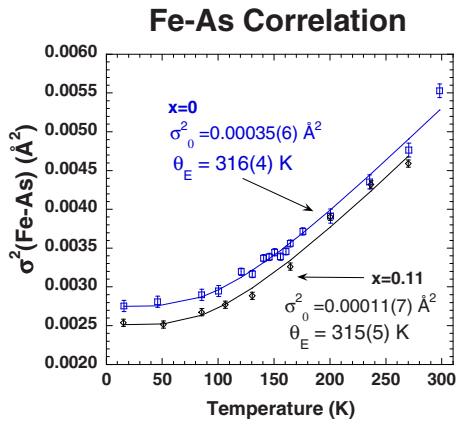

FIG. 2. (Color online) Extracted σ^2(T) for the Fe–As bond for the x=0 and 0.11 samples as the upper and lower curves. Note that the Einstein (θ_E) temperatures are the same for both samples.

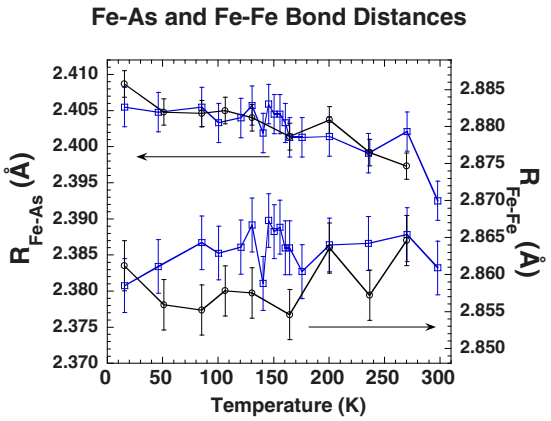

FIG. 4. (Color online) Bond distances for x=0 (blue circles) and x=0.11 (black squares) for the first shell Fe–As distance (upper curves) and second shell Fe–Fe distance (lower curves).

temperature range with a simple two parameter (σ_0^2 and θ_E) model of the vibration of the atom pair. While the effective Einstein temperature for the bond is the same for both the doped and undoped system, there is a decrease in the σ_0^2 static disorder of the bond with F doping.

The Fe–Fe correlations are best modeled with $\sigma_0^2=0$ indicating a very low degree of static disorder with respect to this bond pair (see Fig. 3). While the 11% doped system is fit well over the entire temperature range by an Einstein model, significant variation from this model are found at low temperature for the parent undoped compound. Specifically below ~100 K, a reduction of σ^2 is found for the undoped system. The points fall on the curve for the doped system. The dip in the Fe–Fe thermal factor (Debye–Waller factor, σ^2) for the undoped system near ~100 K corresponds to an enhancement of the Fe–Fe correlations and is possibly a delayed signature of the AFM-SDW which occurs ~145 K. Similar behavior was found near an AFM-SDW ordering temperature was seen in the layered $Ca_3Co_4O_9$ system.[15] Note also that in the region of the structural phase transition (~160 K) no large changes are seen showing that there is no large local distortion in the x=0 system in transiting from the tetragonal to orthorhombic phase. For this Fe–Fe bond, the

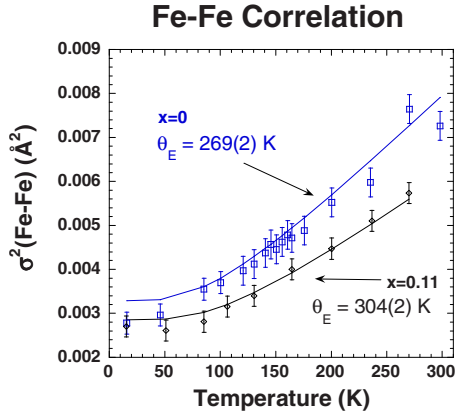

FIG. 3. (Color online) Extracted σ^2(T) for the Fe–Fe bonds for the x=0 and 0.11 samples as the upper and lower curves. Note that the Einstein (θ_E) temperature for this correlation is higher for the doped sample indicating enhanced Fe–Fe coupling with F doping.

Einstein temperature for the doped system is significantly higher than that for the undoped system [304(2) K compared to 269(2) K] suggesting enhanced Fe–Fe interactions with a single model valid over the entire temperature range.

The bond distances of the Fe–As and Fe–Fe shells are plotted as a function of temperature in Fig. 4 as the upper and lower pairs of curves, respectively. As the level of the uncertainties in the measurements no difference is seen between the Fe–As bonds for the doped and undoped systems. For the Fe–Fe bond, on the other hand, possible reduction in the Fe–Fe distance occurs at low temperature. There results are consistent with published neutron diffraction measurements.[3]

To qualitatively understand the Fe–Fe and Fe–As correlations, we show the total charge density (with respect to the orthorhombic unit cell[3] for the parent compound as constant z plots in Figs. 5(a) and 5(b) yielding charge density in the As and Fe layers, respectively. In Figs. 5(c) and 5(d) we plot the charge density for y=0 and 0.25 planes. Note that while the As ions sites are covalently bonded to the Fe sites and also to the neighboring As sites (As–As hybridization) with highly anisotropic charge along bonding directions, the planes containing the Fe ions reveal metallic-like charge distribution with low anisotropy in the regions between the Fe ions [Figs. 5(b) and 5(c)]. Apart from the effect of the small difference in distance between the Fe–As and Fe–Fe bond, the reduced Einstein temperature in the undoped system is possibly due to the weaker bonding in the Fe plane. On a local level this bonding is enhanced at low temperatures suggesting that strong short-range magnetic correlations exist. In the doped system the strong magnetic correlations exist for a broader range of temperatures yielding a higher Fe–Fe Einstein temperature.

To illustrate the effect of F doping, we plot the charge density for the doped supercell in Fig. 6(a) on a log scale (as in Fig. 5) and the difference between the doped and undoped system in Fig. 6(b) for the same charge density section as in Fig. 6(a). Note that doping by F induces changes in the charge density at the Fe sites which may modify the interactions between the Fe ions. No significant changes in charge density is seen on the La, As, or other oxygen sites (not dopant site).

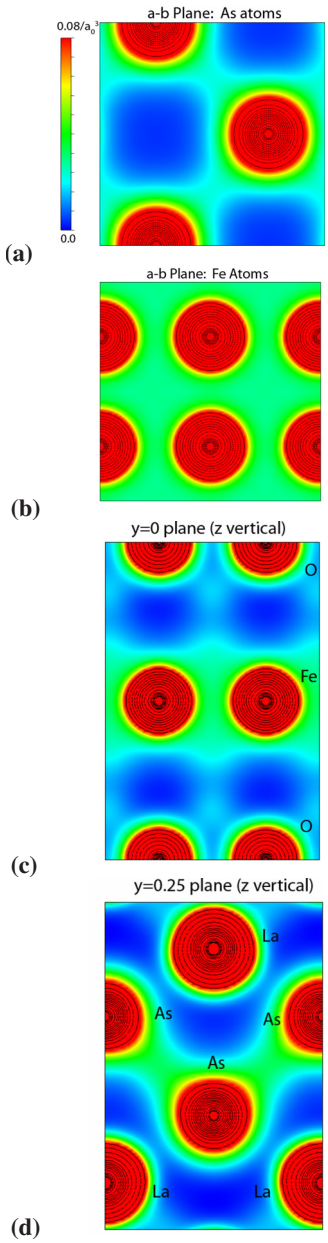

FIG. 5. (Color online) In panels (a) and (b) the change density in the planes for z=0.65 and 0.5 are given showing the charge distribution in the As and Fe layers, respectively. The planes at y=0 and y=0.25 are shown in (c) and (d). All plots have the same z scale [as in (a)] in units of electrons/Bohr radius cubed.

Combining the results, we make the following observations. At the level of the experiments, the doped system is well modeled by Einstein type pair correlations for the Fe–As and Fe–Fe bonds for the entire temperature range. For the undoped system, while the Fe–As bond has a unique effective temperature for entire temperature range, the Fe–Fe bonds are possibly with two distinct regions $T < 100$ K and $T > 100$ K. The primary impact of doping, on the charge density, is a transfer of charge to the Fe layer with an enhancement of the Fe–Fe correlation and reduction of static disorder. The results are consistent with a magnetic correlation origin of superconductivity proposed in theories of these materials (see for example Refs. 16–19).

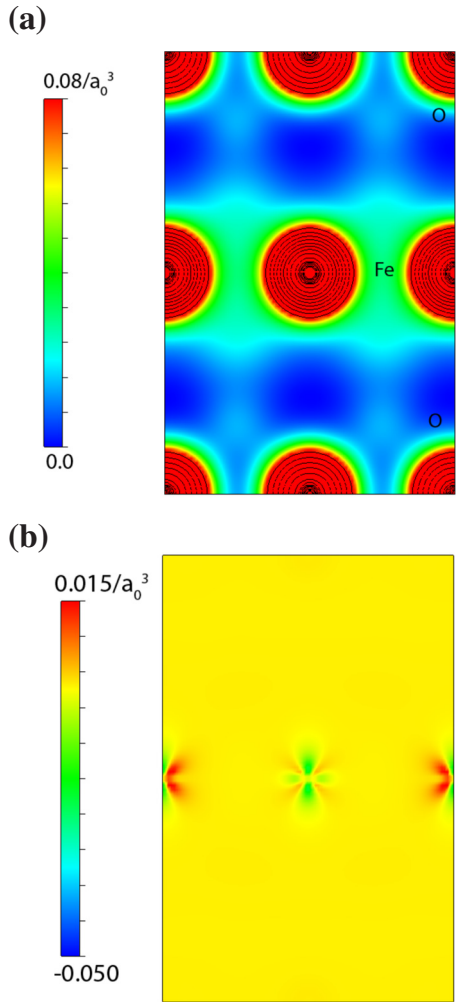

FIG. 6. (Color online) (a) Slice of the total charge density of 12.5% doped model system based on double unit cell revealing the a plane contain the Fe and O ions. Note the similarity in terms of the delocalized charge in the Fe layer with Fig. 4(c). The intensity scale is the same as in Fig. 5. (b)The difference between the total charge density of the F doped and undoped system for the same plane as in (a) showing that the Fe layer is modified by F doping. The yellow background of the figure denotes zero charge density while green and red are negative and positive charge density, respectively.

ACKNOWLEDGMENTS

This work is supported by DOE under Grants Nos. DE-FG02-07ER46402 (NJIT) and DE-FG02-07ER46382 (Rutgers University). Data acquisition was performed at Brookhaven National Laboratory's National Synchrotron Light Source (NSLS) which is funded by the U.S. Department of Energy.

[1]H. Takahashi, K. Igawa, K. Arii, Y. Kamihara, M. Hirano, and H. Hosono, Nature (London) **453**, 376 (2008) (and references therein).
[2]H. Hosono and Z.-A. Ren, New J. Phys. **11**, 025003 (2009); M. V. Sadovskii, Physics Uspekhi **51**, 1201 (2008); I. I. Mazin and J. S. Schmalian, Physica C **469**, 614 (2009); L. Boeri, O. V. Dolgov, and A. A. Golubov, Physica C **469**, 628 (2009); K. Ishida, Y. Nakai, and H. Hosono, J. Phys. Soc. Jpn. **78**, 062001 (2009); J. Dai, Q. Si, J.-X. Zhu, and E. Abrahams, Proc. Natl. Acad. Sci. U.S.A. **106**, 4118 (2009).
[3]Q. Huang, J. Zhao, J. W. Lynn, G. F. Chen, J. L. Luo, N. L. Wang, and P. Dai, Phys. Rev. B **78**, 054529 (2008); C. de la Cruz, Q. Huang, J. W. Lynn, J. Li, W. Ratcliff II, J. L. Zarestky, H. A. Mook, G. F. Chen, J. L. Luo, N. L. Wang, and P. Dai, Nature (London) **453**, 899 (2008); M. McGuire, A. D. Christianson, A. S. Sefat, B. C. Sales, M. D. Lumsden, R. Jin, E. A. Payzant, D. Mandrus, Y. Luan, V. Keppens, V. Varadarajan, J. W. Brill, R.

P. Herman, M. T. Sougrati, F. G. Grandjean, and G. J. Long, Phys. Rev. B **78**, 094517 (2008); T. Yildirim, arXiv:0805.2888v1 (unpublished).
[4]A. Ignatov, C. L. Zhang, M. Vannucci, M. Croft, T. A. Tyson, D. Kwok, Z. Qin, and S.-W. Cheong, arXiv:0808.2134v2 (unpublished).
[5]T. A. Tyson, T. Wu, K. H. Ahn, S.-B. Kim, and S.-W. Cheong, Phys. Rev. B **81**, 054101 (2010).
[6]B. Ravel and M. Newville, J. Synchrotron Radiat. **12**, 537 (2005); *Principles, Applications, Techniques of EXAFS, SEXAFS and XANES*, edited by D. C. Konningsberger and R. Prins (Wiley, New York, 1988).
[7]C. J. Zhang, H. Oyanagi, Z. H. Sun, Y. Kamihara, and H. Hosono, Phys. Rev. B **78**, 214513 (2008).
[8]C. H. Booth and F. Bridges, Phys. Scr., T **115**, 202 (2005).
[9]T. A. Tyson, M. Deleon, S. Yoong, and S. W. Cheong, Phys. Rev. B **75**, 174413 (2007).
[10]A. L. Ankudinov and J. J. Rehr, Phys. Rev. B **56**, R1712 (1997).
[11]T. Nomura, S. W. Kim, Y. Kamihara, M. Hirano, P. V. Sushko, K. Kato, M. Takata, A. L. Shluger, and H. Hosono, Supercond. Sci. Technol. **21**, 125028 (2008).
[12]J. Mustre de Leon, S. D. Conradson, I. Batistić, A. R. Bishop, I. D. Raistrick, M. C. Aronson, and F. H. Garzon, Phys. Rev. B **45**, 2447 (1992).
[13]M. Vaccari and P. Fornasini, J. Synchrotron Radiat. **13**, 321 (2006), and references therein.
[14]K. Schwarz, P. Blaha, and G. K. H. Madsen, Comput. Phys. Commun. **147**, 71 (2002).
[15]T. A. Tyson, Z. Chen, Q. Jie, Q. Li, and J. J. Tu, Phys. Rev. B **79**, 024109 (2009).
[16]Z.-J. Yao, J.-X. Li, and Z. D. Wang, New J. Phys. **11**, 025009 (2009).
[17]I. I. Mazin, D. J. Singh, M. D. Johannes, and M. H. Du, Phys. Rev. Lett. **101**, 057003 (2008).
[18]K. Haule, J. H. Shim, and G. Kotliar, Phys. Rev. Lett. **100**, 226402 (2008).
[19]S. Raghu, X.-L. Qi, C.-X. Liu, D. J. Scalapino, and S.-C. Zhang, Phys. Rev. B **77**, 220503(R) (2008).